# Solidification cells at low velocity: The moving symmetric model

Alain Karma
*California Institute of Technology, Pasadena, California 91125*
(Received 23 May 1986)

This paper is the first in a series of theoretical studies of singular cells in the small solute Peclet number limit ($P \to 0$) of two-dimensional models of directional solidification. In this limit solute diffusion in the frame of the moving front is nearly Laplacian in which case solidification cells and Saffman-Taylor fingers are closely related. Here Langer's moving symmetric model in the absence of temperature gradient (which also describes solidification in a channel of width $\lambda$ at unit undercooling) is considered. A boundary integral equation describing steady-state cells is derived and it is shown that in the $P \to 0$ limit this equation can be expressed in terms of a single dimensionless parameter $\sigma \propto d_0 l / \lambda^2$. The endpoint singularity is studied analytically and physically admissible solutions are found numerically to only exist for a discrete set of values of $\sigma$. The small $P$ dependence of $\sigma$ is also examined.

## I. INTRODUCTION

The problem of pattern selection in interfacial nonequilibrium systems has received an increasing amount of theoretical and experimental interest. In particular dendritic crystals[1-6] and viscous fingers in Hele-Shaw cells[7-12] have been the subject of numerous studies. These studies have shown numerically and more recently analytically that pattern selection in both systems is controlled by surface tension. Capillary forces break the continuum of steady-state solutions (Ivantsov family of needle crystals or Saffman-Taylor family of fingers), yielding a discrete set of solutions among which only one is generally stable and relevant in experiment. This selection criterion can be expressed in terms of a nonlinear solvability condition which corresponds to the requirement that physically admissible steady-state interfaces remain smooth at the tip of the cell. In dendritic solidification the presence of some form of crystalline anisotropy, either static or kinetic, is essential for this discrete set of solutions to be nonempty (at least in 2D), while in viscous fingering such inclusion is not necessary, the nearby channel walls playing a role similar to crystalline anisotropy.

Let us now group in, say, class 1 those interfacial patterns for which a discrete set of solutions of the steady-state equations exists for given values of the external parameters (undercooling, applied pressure gradient,...) and in class 2 those patterns for which a family of solutions exist. Clearly, crystal dendrites and Saffman-Taylor fingers fall within class 1. However, what is not so clear at this point is to what extent this class is universal and encompasses other interfacial patterns of theoretical and experimental interest. In particular, does directional solidification fall within class 1? To examine this question let us differentiate between two different kinds of steady-state cellular interfaces which can occur in directional solidification: (1) small amplitude cells and (2) (quasi-infinite amplitude) singular cells or solidification "fingers" which have been observed experimentally at relatively slow solidification rates.[13-15] With regard to small amplitude cells, numerous theoretical studies[16-20] have already shown that these states can exist near threshold of the planar instability (Mullins-Sekerka instability) within a continuous band of wave numbers, their slow dynamics being described by an amplitude equation similar in form to the equation of Newell and Whitehead,[21] and Segel,[22] for convective cells. Thus, the cell spacing in an array of small amplitude solidification cells or an array of convective cells (as opposed to the tip radius of a needle crystal or the width of a viscous finger) is left undetermined by the steady-state equations, and these states fall within class 2. However, for singular cells, the existence property of steady-state solutions has not yet been established. In previous work, deep cells were found numerically[23] at half the critical wave number (where the planar instability first occurs) but the problem of cell-spacing selection was not examined. Other attempts[24,25] were based on small amplitude expansion in the interface displacement, either in real or Fourier space, which by the nature of the expansion can not describe properly singular solutions (infinite amplitude states). These attempts, despite their own merits, thus failed to establish on a firm basis the existence of singular solutions in fully nonlocal models of directional solidification.

In this series of two papers we investigate this question of pattern selection in an array of solidification fingers. For this purpose we adopt the following strategy. We first investigate the simplest nontrivial nonlocal model of directional solidification which exhibits singular cells, and progressively incorporate complicating features of a more realistic model which, hopefully, finally leads us to a relatively accurate description of the experimental system. The advantage of this procedure, over starting immediately with a complicated model, is that we gain a systematic understanding of which complicating features are crucial, in that they alter significantly the existence properties of singular solutions and which ones are unimportant, in that they only have quantitative effects. Note that a similar strategy has been used in the past in the study of small amplitude states.[17-19] Following this path, we first study

 

Langer's moving symmetric model in the absence of temperature gradient (model A). The reason for neglecting the temperature gradient is that its presence destroys the existence of steady-state singular cells in a symmetric model of directional solidification. With infinite cusp singularities and a temperature gradient present simultaneously, overall solute conservation demands that infinite lateral solute concentration gradients be present in the solid, a situation which clearly cannot occur if solute diffusion is allowed in the solid. Therefore model A is the simplest nontrivial mathematical structure which, as we shall see, exhibits at finite surface tension a discrete set of singular spatially periodic solutions.

We emphasize that in first studying singular cells in the absence of a temperature gradient we cannot investigate the effects of the coupling between the solute and temperature fields. This important coupling is responsible for fixing the absolute position of the interface in the frame of the moving front (i.e., the position along an axis parallel to the direction of motion of the front), and, in its absence, this position is left arbitrary. Also, in the absence of this coupling, long-wavelength perturbations are likely to be unstable and alter significantly the global stability of the pattern. Consequently, in the context of model A, our study is restricted to the existence properties of steady-state solutions. Additional questions of stability and the effects of this coupling can be best studied in the context of the more realistic, but mathematically more complex, one-sided model of directional solidification in the presence of a temperature gradient (model B). The steady-state singular solutions of this model will be investigated in part II. There we shall find that the presence of the temperature gradient by itself does not affect the qualitative structure of the problem (in this respect models A and B are very similar), but that the coupling between the interface and the temperature gradient via the miscibility gap, which is strongest for small partition coefficient, has profound qualitative effects (in this respect models A and B differ significantly). Results for model B with unit partition coefficient have been published in Ref. 26.

Finally let us note that although here we have introduced model A as a starting point to a systematic investigation of directional solidification, this model also describes solidification fingers in a channel of width $\lambda$ at unit undercooling (where overall heat or solute conservation requires that the asymptotic width of the finger equals the width of the channel). Clearly, this is because solving the steady-state equations with periodic boundary conditions (BC's) within one "unit cell" or solving them with zero-flux BC's along the normal to the walls are completely equivalent tasks. In this respect, apart from diffusion in the solid which does not have a direct analog in the Saffman-Taylor problem, there is a clear connection between viscous fingers in the limit where they fill the channel (the limit of large surface tension) and the singular solutions of model A in the small Peclet number limit. This connection will be explored in more detail in the following sections.

The scheme of this paper is as follows. In Sec. II we introduce model A and derive a closed integral equation for steady-state cells in the small-$P$ limit. In Sec. III we analyze analytically the endpoint singularity of steady-state solutions (i.e., the cusp region). Section IV contains the details of the numerical solution of the integral equation derived in Sec. II. Our results are then discussed in Sec. V, and finally concluding remarks are included in Sec. VI.

## II. INTEGRAL EQUATION FOR STEADY-STATE CELLS

A complete description of the moving symmetric model of directional solidification can be found in Ref. 18. We now review briefly the model and its starting equations. We study the model in the absence of temperature gradient and restrict our attention to steady-state spatially periodic interfaces of wavelength (cell spacing) $\lambda$. Consider a two-phase system ($\alpha$ and $\beta$ phase) and a solidification front moving at constant velocity $v$ in the $+z$ direction; $\alpha$ and $\beta$ denote the liquid and solid phases respectively, with $C_\alpha$ and $C_\beta$ defined as the equilibrium solute concentrations in each phase at some reference temperature $T_0$. We introduce the solute field

$$\varphi(p)=\frac{1}{P}\left[\frac{C(p)-C^0}{\Delta C^0}\right], \tag{2.1}$$

where

$$P=\frac{2\lambda}{l} \tag{2.2}$$

is the solute Peclet number, $l=(2D/v)$ is the solute diffusion length, $D$ is the coefficient of solute diffusivity which is taken to be equal in the $\alpha$ and $\beta$ phases, $C(p)$ is the solute concentration at points $p=(x,z)$, where $(x,z)$ represents a coordinate system moving at velocity $v$ with the solidification front, $C^0$ is equal to $C_\alpha$ or $C_\beta$ in the $\alpha$ or $\beta$ phase respectively, and $\Delta C^0 \equiv C_\alpha - C_\beta$ is the miscibility gap assumed to be a constant independent of temperature and local curvature of the interface. Note that we have introduced the solute field $\varphi(p)$ in place of the field $u(p)\equiv C(p)-C^0$ used previously in Ref. 18. This choice has been made to facilitate the discussion of the small-$P$ limit where $\varphi(p)$ is the direct analog of the pressure field in Saffman-Taylor fingering. Here $\varphi(p)$ obeys the steady-state diffusion equation in the frame of the moving front,

$$\nabla^2\varphi+P\frac{\partial\varphi}{\partial z}=0, \tag{2.3}$$

the condition of mass conservation at the interface,

$$\cos\theta_n=-\hat{n}\cdot[(\nabla\varphi)_\alpha-(\nabla\varphi)_\beta]_{\text{int}}, \tag{2.4}$$

and the condition of local thermodynamic equilibrium at the interface (Gibbs-Thomson relation) which in the absence of temperature gradient takes the simple form

$$(\varphi)_{\text{int}}=-\frac{2V}{P^2}\kappa(\zeta). \tag{2.5}$$

All lengths are measured in units of $\lambda$, $\theta_n$ is the angle between the local normal and the $z$ axis,

$$\kappa(\zeta)=-\frac{d^2\zeta}{dx^2}\left[1+\left[\frac{d\zeta}{dx}\right]^2\right]^{-3/2}$$

is the local curvature of the interface, where $\zeta(x)\equiv(z)_{\rm int}$ denotes the position of the interface, and we have introduced the dimensionless surface tension or velocity,

$$V=\frac{d_0}{l} \tag{2.6}$$

where $d_0$ is the capillary length. Finally the solute concentration far ahead of the moving interface, $C_\infty$, is chosen equal to $C_\beta$ which implies

$$\varphi_\infty\equiv\varphi(z=+\infty)=-\frac{1}{P}\ . \tag{2.7}$$

Here (2.7) is equivalent to the condition of unit undercooling, $\Delta=1$, where

$$\Delta=(C_a-C_\infty)/\Delta C^0$$

is the direct analog of the thermal undercooling

$$\Delta=(T_M-T_\infty)/(L/c_p)$$

which measures the difference between the melting temperature and the temperature at infinity in units of the ratio of the latent heat to the specific heat. Also note that $C_\infty=C_\beta$ requires that the width of the liquid region in between the solidification fingers shrinks to zero infinitely far down in the cusps ($z\to-\infty$). This must be so since overall solute conservation demands that the total amount of impurities far ahead of the interface be absorbed in the $\beta$ phase as the solidification front progresses.

Next we wish to investigate the existence of singular solutions of the steady-state equations (2.3)–(2.5) and BC's (2.7). This investigation is best carried out by recasting [(2.3)–(2.5) and (2.7)] into a closed integral equation for the interface, then analyzing analytically the endpoint singularity (cusp region), and finally solving numerically this integral equation making use of the known analytical behavior of the endpoint. Before describing these steps in detail, we first discuss qualitatively the limiting form of the steady-state equations for $P\ll1$ using the analogy with the Saffman-Taylor problem. Our hope here is to provide some physical intuition for the small-$P$ limit and the connection between the two problems before plunging directly in a more mathematical analysis.

The steady-state equations describing viscous fingering in a Hele-Shaw cell,[7] in the absence of a gravitational field, differ from the ones of the present model in the following way. The analog of (2.3) is simply the Laplacian, the $P\partial_z\varphi$ term being absent. The term $(\nabla\varphi)_\beta$ does not appear in the equation corresponding to (2.4), the analog of diffusion in the solid being absent in viscous fingering. The analog of the Gibbs-Thomson relation is identical in form to (2.5) apart from a trivial renaming of the effective surface tension ($2V/P^2$). Finally the analog of the BC's (2.7) is simply the constant gradient BC's $(\partial_z\varphi)_\infty=$ const corresponding to uniform fluid flow far ahead of the finger. To probe the connection between the two problems further consider the spatial variations of the solute field $\varphi(p)$ far ahead of a solidification front consisting of an array of cells. The asymptotic form of $\varphi(p)$ for $z\gg0$ can be obtained by simply replacing the array of cells by a constant potential plane: $\varphi(x,z=0)=0$ and solving (2.3)–(2.5) and (2.7) accordingly. We obtain

$$\varphi(z)\simeq\frac{e^{-Pz}-1}{P}\quad\text{for } z\gg0 \tag{2.8a}$$

or

$$\varphi(z)\simeq-z\quad\text{for } \frac{1}{P}\gg z\gg0\ . \tag{2.8b}$$

The structure of (2.8a) and (2.8b) then suggests that, in the $P\to0$ limit, we might be able to replace the BC's (2.7) by the constant gradient BC's $(\partial_z\varphi)_\infty=-1$. Furthermore in the tip region the spatial variations of $\varphi$ are of order one and we might neglect the $P\partial_z\varphi$ term in (2.3). At the end of this section we shall demonstrate that such procedures are indeed correct. Thus, in the $P\to0$ limit, the steady-state equations for the two problems are almost identical, the difference arising solely from (2.4) (diffusion in the $\beta$ phase), and all $P$ dependence is contained in the effective surface tension ($2V/P^2$).

We now turn to the integral formulation of the steady-state (2.3)–(2.5) and (2.7) for a periodic array of cells. We study a single cell over the interval $x=[0,1]$, with the two endpoint singularities at $x=0$ and $x=1$, and impose periodic BC's. The appropriate integral equation is then (Ref. 18)

$$-\frac{2V}{P^2}\kappa(\zeta)=\varphi_\infty+\int_0^1 dx'\,G(\Delta x,\Delta\zeta)\ , \tag{2.9}$$

where $\Delta x=x-x'$, $\Delta\zeta=\zeta(x)-\zeta(x')$, and $G(x-x',z-z')$ satisfies

$$\left[\nabla'^2-P\frac{\partial}{\partial z'}\right]G=-\delta(x-x')\delta(z-z')\ , \tag{2.10}$$

with periodic BC's. To derive an expression for $G$ we substitute the form

$$G=\sum_{n=-\infty}^{\infty}\int_{-\infty}^{\infty}dq\,e^{i2\pi n(x-x')+iq(z-z')}G_n(q) \tag{2.11}$$

into (2.10), calculate the inverse Fourier transform, and evaluate the resulting expression on the interface [i.e., $z-z'\to\zeta(x)-\zeta(x')$]. We obtain the exact expression for $G$,

$$G(\Delta x,\Delta\zeta)=\frac{1}{P}e^{-P(|\Delta\zeta|+\Delta\zeta)/2}+\frac{e^{-P\Delta\zeta/2}}{4\pi}\sum_{n=1}^{\infty}\frac{\exp(2\pi n\{i\Delta x-|\Delta\zeta|[1+(P/4\pi n)^2]^{1/2}\})}{n[1+(P/4\pi n)^2]^{1/2}}+\text{c.c.} \tag{2.12}$$

In the small-$P$ limit the square-root term in (2.12) can be replaced by unity and the resulting sum over $n$ can then be expressed exactly in terms of a logarithm. The small-$P$ expression for $G$ then becomes

$$\tilde{G}(\Delta x,\Delta\zeta)=\frac{1}{P}e^{-P(|\Delta\zeta|+\Delta\zeta)/2}-\frac{e^{-P\Delta\zeta/2}}{4\pi}\ln\Lambda^{+} \quad \text{for } \left[\frac{P}{4\pi}\right]^2\ll 1 , \tag{2.13a}$$

$$\Lambda^{\pm}=1+e^{-4\pi|\Delta\zeta|}-2e^{-2\pi|\Delta\zeta|}\cos[2\pi(x\mp x')] . \tag{2.13b}$$

Using (2.7), we then rewrite (2.9) in the form

$$-2\sigma\kappa(\zeta)=\int_0^1 dx'\left[\tilde{G}(\Delta x,\Delta\zeta)-\frac{1}{P}\right], \tag{2.14}$$

where we have defined

$$\sigma=\frac{V}{P^2}=\frac{d_0 l}{4\lambda^2} . \tag{2.15}$$

Let us now examine the $P\to 0$ limit of (2.14). If we can bring this limit under the integral sign and simply expand the integrand, then (2.14) can be rewritten

$$-2\sigma\kappa(\zeta)=\int_0^1 dx'\,G_L(\Delta x,\Delta\zeta)+O(P)+\cdots , \tag{2.16}$$

where

$$G_L(\Delta x,\Delta\zeta)=\lim_{P\to 0}\left[\tilde{G}(\Delta x,\Delta\zeta)-\frac{1}{P}\right]=-\tfrac{1}{2}(|\Delta\zeta|+\Delta\zeta)-\frac{1}{4\pi}\ln\Lambda^{+} \tag{2.17}$$

is the Green's function for the free Laplacian with a constant external field BC's. Thus, if the above limiting procedure is valid and we neglect terms of order $P^n$ $(n\geq 1)$, (2.16) is indeed the integral equation corresponding to the steady-state equations (2.3)–(2.5) and (2.7) with (2.3) replaced by the free Laplacian and (2.7) by the uniform gradient BC's $(\partial_z\varphi)_\infty=-1$, in agreement with the physical arguments presented earlier. To prove the validity of this limiting procedure let us rewrite (2.14) in the form

$$-\sigma\kappa(\zeta)=-\int_0^{1/2}\frac{dx'}{8\pi}e^{-P\Delta\zeta/2}(\ln\Lambda^{+}+\ln\Lambda^{-})+\int_0^{x(\zeta)}dx'\left[\frac{e^{-P\Delta\zeta}-1}{P}\right], \tag{2.18}$$

where we have combined (2.14) with (2.13a) and (2.13b) and used the reflection symmetry about $x=\frac{1}{2}$: $\zeta(x)=\zeta(1-x)$ to restrict our domain of integration to $x=[0,\frac{1}{2}]$: $x(\zeta)$ denotes the interface with $x$ as function of $\zeta$. We then change the integration variable from $x'=x(\zeta')$ to $\zeta'=\zeta(x')$ which maps the interval $x'=[0,\frac{1}{2}]$ to $\zeta'=[-\infty,\zeta_{\rm tip}]$ for singular cells and rewrite (2.18) in the form

$$-\sigma\kappa(\zeta)=-\frac{1}{8\pi}\int_{-\infty}^{\zeta_{\rm tip}}d\zeta'\frac{dx'}{d\zeta'}e^{-P\Delta\zeta/2}(\ln\Lambda^{+}+\ln\Lambda^{-})+\int_{-\infty}^{\zeta}d\zeta'\frac{dx'}{d\zeta'}\left[\frac{e^{-P\Delta\zeta}-1}{P}\right] . \tag{2.19}$$

First consider the first term on the rhs (right-hand side) of (2.19). From (2.13a) and (2.13b) it follows that $\ln\Lambda^{\pm}$ decays exponentially in $|\Delta\zeta|$ on a length scale of order one and consequently $e^{-P\Delta\zeta/2}$ can be expanded in a Taylor series in $P\Delta\zeta$. Next the integrand of the second term on the rhs of (2.19) can be expanded in a Taylor series in $P\Delta\zeta$ only if $(dx'/d\zeta')$ decays to zero much faster than $e^{P\zeta'}$ as $\zeta'\to-\infty$. In Sec. III we shall analyze the endpoint singularity at $x=0$ and find that asymptotically $(dx'/d\zeta')\sim e^{t\zeta'}$, where $t$ is related to $\sigma$ by the transcendental equation $(1/2t^2)\cot(t/2)=\sigma$; $\sigma$ is in turn determined by the requirement that singular solutions of (2.19) exist (the inner-outer matching condition). Furthermore in solving (2.19) [or equivalently (2.18)] numerically we shall find that singular solutions exist for a discrete set of values of $\sigma$: $\sigma_1>\sigma_2>\sigma_3\cdots$, with the corresponding values of $t$: $t_1,t_2,t_3,\ldots$, of order one. Thus, the integrand of the second term on the rhs of (2.19) can be expanded in powers of $P\Delta\zeta$. Neglecting terms of order $P^n$ $(n\geq 1)$ [Eq. (2.18)] can then safely be rewritten in the form

$$-\sigma\kappa(\zeta)=-\int_0^{1/2}\frac{dx'}{8\pi}(\ln\Lambda^{+}+\ln\Lambda^{-})-\int_0^{x(\zeta)}dx'\,\Delta\zeta \tag{2.20}$$

which is valid for $V=\sigma P^2\ll 1$. Equation (2.20) is the analog for solidification fingers of the small undercooling equation of Pelcé and Pomeau[26] for dendritic crystals, the condition of small growth velocity—$V\ll 1$—playing the role of the small undercooling condition—$\Delta\ll 1$. The cell spacing $\lambda$ is quantized and given by

$$\lambda_i=\frac{1}{2}\left[\frac{d_0 l}{\sigma_i}\right]^{1/2}, \quad i=1,2,\ldots, \tag{2.21}$$

where the $P$-independent $\sigma_i$'s are determined by (2.20) and the $P$ dependence of the $\sigma_i$'s for $[P/4\pi]^2\ll 1$ is determined by (2.18). Finally, let us note that at zero surface tension $(\sigma=0)$ the interface is a line of constant $\varphi$ (i.e., $\varphi=0$) which implies that $\varphi$ must be constant inside the solid and therefore $(\nabla\varphi)_\beta=0$ in (2.4). Thus, the $\sigma=0$ solution of (2.20) must be the limit where the finger fills the channel of the zero surface tension Saffman-Taylor family of steady-state fingers, namely, the planar interface.

## III. ENDPOINT SINGULARLY

To analyze the endpoint singularity at $x=0$ $(\zeta\to-\infty)$ we first rewrite (2.18) in the form

$$-\sigma\frac{d^2x}{d\zeta^2}-\int_{-\infty}^{\zeta}d\zeta'\frac{dx'}{d\zeta'}\left[\frac{e^{-P\Delta\zeta}-1}{P}\right]=R(\zeta) , \tag{3.1}$$

where we have used the asymptotic form of the curvature $\kappa(\zeta)=(d^2x/d\zeta^2)$ for $(dx/d\zeta)^2\ll 1$ and defined

$$R(\zeta)=-\frac{1}{8\pi}\int_{-\infty}^{\zeta_{\rm tip}}d\zeta'\frac{dx'}{d\zeta'}e^{-P\Delta\zeta/2}(\ln\Lambda^{+}+\ln\Lambda^{-}) . \tag{3.2}$$

We start our analysis from (2.18) to demonstrate explicitly that for $P\ll 1$ the asymptotic behavior of the solution

near the singularity point is independent of $P$, except through $\sigma$, thereby verifying the validity of (2.20) derived in Sec. II. Differentiating (3.1) with respect to $\zeta$ we obtain

$$-\sigma\frac{d^3x}{d\zeta^3}+\int_{-\infty}^{\zeta}d\zeta'\frac{dx'}{d\zeta'}e^{-P\Delta\zeta}=\frac{dR}{d\zeta}\ . \tag{3.3}$$

Then eliminating the second term on the lhs (left-hand side) of (3.3) via (3.1) and simply noting that $\int_{-\infty}^{\zeta}d\zeta'(dx'/d\zeta')=x(\zeta)$, (3.3) can be written in the form

$$x(\zeta)-\sigma\frac{d^3x}{d\zeta^3}-\frac{dR}{d\zeta}=P\left[\sigma\frac{d^2x}{d\zeta^2}+R(\zeta)\right]\ . \tag{3.4}$$

Next to evaluate $R(\zeta)$ we assume a simple exponential asymptotic solution of the form

$$x(\zeta')=x(\zeta)e^{-t\Delta\zeta} \tag{3.5}$$

(recall $\Delta\zeta=\zeta-\zeta'$) and substitute (3.5) in (3.2). Using the definition of $\Lambda^{\pm}$ (2.13b) with $\cos2\pi(x\pm x')\simeq1$ for $x$, $x'\sim0$ (3.2) becomes

$$R(\zeta)=-\frac{tx(\zeta)}{2\pi}\int_{-\infty}^{\zeta_{\rm tip}}d\zeta'\,e^{-t\Delta\zeta}\ln(1-e^{-2\pi|\Delta\zeta|})+O(P)\ . \tag{3.6}$$

Then, changing the integration variable from $\zeta'$ to $w\equiv-2\pi\Delta\zeta$, (3.6) can be written

$$R(\zeta)=-\frac{tx(\zeta)}{(2\pi)^2}\int_{-\infty}^{2\pi(\zeta_{\rm tip}-\zeta)}dw\,e^{(t/2\pi)w}\ln(1-e^{-|w|})\ . \tag{3.7}$$

In the asymptotic region $-\zeta\gg1$ and the upper bound of integration in (3.7) can be replaced by $+\infty$ as long as $(t/2\pi)<1$. Then combining (3.4), (3.5), and (3.7) we obtain

$$1-\sigma t^3-\frac{t^2}{4}[g(t)+g(-t)]=0 \tag{3.8}$$

for $P\ll1$ and $t<2\pi$ where we have defined

$$g(t)=-\frac{1}{\pi^2}\int_0^{\infty}dw\,e^{(t/2\pi)w}\ln(1-e^{-w})\ . \tag{3.9}$$

To evaluate $g(t)+g(-t)$ we change the integration variable in (3.9) from $w$ to $y=e^{-w}$, (3.9) then becomes

$$g(t)=-\frac{1}{\pi^2}\int_0^1dy\,y^{-(t/2\pi)-1}\ln(1-y)\ , \tag{3.10}$$

where (3.10) is tabulated in Ref. 27 and

$$g(t)+g(-t)=\frac{1-\frac{t}{2}\cot\left[\frac{t}{2}\right]}{\left[\frac{t}{2}\right]^2}\ . \tag{3.11}$$

Finally combining (3.8) and (3.11) we obtain that $t$ is determined by the roots of the transcendental equation

$$\frac{1}{2t^2}\cot\left[\frac{t}{2}\right]=\sigma\quad\text{for } P\ll1,\ \ t<2\pi \tag{3.12}$$

where the asymptotic behavior of solutions near the endpoint is a simple exponential given by (3.5).

## IV. NUMERICAL TREATMENT

In this section we present the details of our numerical treatment of the integrodifferential equation (2.18). We start from (2.18) rather than (2.20) in order to include in our calculations the small $P$ dependence of $\sigma$; $\sigma$ corresponding to (2.20) is then the $P\to0$ limit of $\sigma(P)$. The method we use is very similar to the one used previously in numerical studies of Saffman-Taylor fingers[8,9] and dendritic crystals.[4,5] Its essence is to represent the interface by $N$ grid points and solve the set of nonlinear equations defined by (2.18) with an $N$-dimensional Newton method.

### A. Parametrization of the interface

Because of the endpoint singularity at $x=0$, $\zeta(x)$ does not provide an adequate parametrization of the interface. Using $x(\zeta)$ instead and rewriting (2.18) in the form (2.19) removes the singularity at $x=0$ but introduces a new singularity at the tip ($x=\frac{1}{2}$). To remove these difficulties we parametrize the interface by a polar-coordinate system in the tip region and $x(\zeta)$ in the cusp region, thereby removing singularities at both endpoints simultaneously. A similar parametrization has been used previously in Ref. 23. The interface is broken up in three regions. Region I is delimited by $\zeta_l\le\zeta\le\zeta_{\rm tip}$ and described by a polar coordinate system $r(\theta)$ where $\theta$ varies from 0 to $(\pi/2)$ as $\zeta$ varies from $\zeta_l$ to $\zeta_{\rm tip}$. The origin of $r(\theta)$ is at $(x=\frac{1}{2}, z=\zeta_l)$ and the interface is then defined parametrically by $x(\theta)=\frac{1}{2}-r(\theta)\cos\theta$ and $\zeta(\theta)=\zeta_l+r(\theta)\sin\theta$. Region II is delimited by $\zeta_l\le\zeta\le\zeta_l$ and parametrized by $r(\zeta)=\frac{1}{2}-x(\zeta)$. This choice is equivalent to parametrizing the interface by $x(\zeta)$ and $r(\zeta)$ is introduced such that the variable $r$ is continuous at the junction between regions I and II [i.e., $r(\zeta_l)=r(\theta=0)$]. The interface in region I + II is discretized with $n$ grid points, $l$ equally spaced points in $\zeta$, and $n-l+1$ equally spaced points in $\theta$ [note that although $(n-l+1)+(l)=n+1$ there are only $n$ grid points since the grid point at $\theta=0$, $\zeta=\zeta_l$ is common to both regions]. Let us define $b=\zeta_l-\zeta_1$, $h_2=[b/(l-1)]$, and $h_1=[\pi/2(n-l)]$. Then for $l\le i\le n$

$$\begin{aligned}\theta_i&=(i-l)h_1\ ,\\ r_i&=r(\theta_i)\ ,\\ x_i&=\tfrac{1}{2}-r_i\cos\theta_i\ ,\\ \zeta_i&=\zeta_l+r_i\sin\theta_i\ ,\end{aligned} \tag{4.1}$$

and for $1\le i\le l$

$$\begin{aligned}\zeta_i&=\zeta_1+(i-1)h_2\ ,\\ r_i&=r(\zeta_i)\ ,\\ x_i&=\tfrac{1}{2}-r_i\ .\end{aligned} \tag{4.2}$$

Region III is delimited by $-\infty\le\zeta\le\zeta_1$ which, following

the analysis of Sec. III, we describe by an exponential form

$$x(\zeta)=x_1 e^{t(\zeta-\zeta_1)}, \tag{4.3}$$

where $t$ is determined by the matching condition

$$t=\frac{1}{h_2}\ln\left[\frac{x_2}{x_1}\right]. \tag{4.4}$$

The value of $t$ determined by (4.4) can then be compared with the analytical prediction (3.12) as a self-consistency check.

### B. Discretization of the integral equation and the logarithmic singularities

Next we rewrite integral equation (2.18) in the form

$$\int_{-\infty}^{\zeta_1} d\zeta \frac{dx(\zeta)}{d\zeta}\Gamma(x_i,x(\zeta);\zeta_i-\zeta)+\sum_{j=1}^{n-1} I_i^j+\sigma\kappa_i=0, \tag{4.5}$$

where $\kappa_i$ is the curvature at $(x_i,\zeta_i)$ and we have defined

$$I_i^j=\int_{q_j}^{q_{j+1}} dq \frac{dx(q)}{dq}\Gamma(x_i,x(q);\zeta_i-\zeta(q)) \tag{4.6}$$

with in region II

$$q=\zeta(q),\quad q_j=\zeta_j,\quad \text{for } 1\le j\le l-1$$

and in region I

$$q=\theta,\quad q_j=\theta_j,\quad \text{for } l\le j\le n. \tag{4.7}$$

$\Gamma$ is the integrand of (2.18)

$$\Gamma(x,x';\Delta\zeta)=L(x,x';\Delta\zeta)+E(\Delta\zeta) \tag{4.8a}$$

with $\Delta\zeta=\zeta_i-\zeta$,

$$L(x,x';\Delta\zeta)\equiv-\frac{e^{-P\Delta\zeta/2}}{8\pi}(\ln\Lambda^+ +\ln\Lambda^-) \tag{4.8b}$$

and

$$E(\Delta\zeta)\equiv\frac{e^{-P(|\Delta\zeta|+\Delta\zeta)/2}-1}{P}. \tag{4.8c}$$

The first term on the lhs of (4.5) represents the part of the integration over region III where $x(\zeta)$ is given by (4.3). To evaluate this integral we first evaluate analytically the contribution from $E(\Delta\zeta)$. This contribution is simply

$$Q(\zeta_i)=x_1 t\int_{-\infty}^{\zeta} d\zeta' e^{t(\zeta'-\zeta_1)}E(\zeta_i-\zeta')$$
$$=\frac{x_1}{Pt(P+t)}[-Pt+t^2(e^{-P(\zeta_i-\zeta_1)}-1)]. \tag{4.9}$$

Next we map the interval $\zeta=[-\infty,\zeta_1]$ to the interval $y=[-1,1]$ by the rational transformation

$$\zeta(y)=\frac{2\zeta_1}{1+y}\quad(\zeta_1<0)$$

and change the integration variable from $\zeta$ to $y$. The contribution from $L(x_i,x(\zeta);\zeta_i-\zeta)$ is then

$$R(x_i,\zeta_i)=-2\zeta_1 x_1 t\int_{-1}^{1} dy\frac{1}{(1+y)^2}e^{t[\zeta(y)-\zeta_1]}L(x_i,x_1 e^{t[\zeta(y)-\zeta_1]};\zeta_i-\zeta(y)), \tag{4.10}$$

where (4.10) is evaluated by standard Gauss-Legendre quadrature with 20 points (which was found sufficient to provide good accuracy). Equation (4.5) then becomes

$$Q(\zeta_i)+R(x_i,\zeta_i)+\sum_{j=1}^{n-1} I_i^j+\sigma\kappa_i=0. \tag{4.11}$$

To evaluate $I_i^j$ defined by (4.6) we need expressions for $x(q)$ and $\zeta(q)$ within each interval $q_j\le q\le q_{j+1}$. For this purpose we represent $r(q)$ by a Taylor series in $(q-q_j)$ truncated at third order

$$r(q)=r_j+\sum_{m=1}^{3}\frac{1}{m!}r_j^{(m)}(q-q_j)^m,\quad q_j\le q\le q_{j+1} \tag{4.12}$$

where the derivatives

$$r_j^{(m)}=\left[\frac{d^m r(q)}{dq^m}\right]_{(x_j,\zeta_j)} \tag{4.13}$$

are evaluated by central differences in terms of $(r_{j+2},r_{j+1},r_j,r_{j-1},r_{j-2})$ and $h_1$ in region I, or $h_2$ in region II. (At the boundary points between I and II modified central difference expressions are derived to account for unequal grid spacing, $h_1$ and $h_2$ appearing simultaneously.) Then $x(q)$ and $\zeta(q)$ appearing in (4.6) are related to $r(q)$ by $x(q)=\frac{1}{2}-r(q)$, $\zeta(q)=q$, in region II, and $x(q)=\frac{1}{2}-r(q)\cos q$, $\zeta(q)=\zeta_l+r(q)\sin q$, in region I. The integrable logarithmic singularities appearing in $I_i^i$ and $I_i^{i-1}$ are then subtracted and evaluated analytically within the intervals $q_i\le q\le q_{i+1}$ and $q_{i-1}\le q\le q_i$, respectively. Following the scheme developed by Meiron in Ref. 4 the logarithmic part of $I_i^i$

$$-\int_{q_i}^{q_{i+1}}\frac{dq}{8\pi}e^{-(P/2)[\zeta_i-\zeta(q)]}\frac{dx(q)}{dq}[\ln\Lambda^+ +\ln\Lambda^-] \tag{4.14}$$

is rewritten in the form

$$-\int_{q_i}^{q_{i+1}}\frac{dq}{8\pi}[a_i+b_i(q-q_i)+c_i(q-q_i)^2][\ln\Lambda^+ -\ln(q-q_i)^2+\ln\Lambda^-]-\frac{1}{4\pi}S_i, \tag{4.15}$$

where

$$S_i=\left[a_ih+\frac{b_ih^2}{2}+\frac{c_ih^3}{3}\right]\ln h-\left[a_ih+\frac{b_ih^2}{4}+\frac{c_ih^3}{9}\right] \tag{4.16}$$

and $h=h_1$ or $h_2$ in regions I or II respectively. The coefficients $a_i$, $b_i$, and $c_i$ are evaluated in terms of $r_i^{(m)}$ in region II and $r_i$, $r_i^{(m)}$, $\cos q_i$, $\sin q_i$ in region I, by Taylor-series expansion of

$$\frac{dx(q)}{dq}e^{-P[\zeta_i-\zeta(q)]/2}$$

about $q_i$. A similar procedure can then be used to subtract the singularity in $I_i^{i-1}$ for arbitrary $i$ and (4.10) for $i=1$. Also note that $\ln\Lambda^-$ is nonsingular except in the interval $q_{n-1}\le q\le q_n$ when $q_i=q_n$ (i.e., $x+x'\to 0$). Therefore in evaluating $I_n^{n-1}$ the log singularities of $\ln\Lambda^+$ and $\ln\Lambda^-$ need to be removed simultaneously. Finally the $I_i^j$'s are calculated by standard Gauss-Legendre quadrature with two or four points within each interval $q_j\le q\le q_{j+1}$, and $\kappa_i$ is given by

$$\kappa_i=-\frac{r_i^{(2)}}{[1+(r_i^{(1)})^2]^{3/2}} \tag{4.17}$$

in region II and

$$\kappa_i=-\frac{\zeta_i^{(2)}}{[1+(\zeta_i^{(1)})^2]^{3/2}} \tag{4.18a}$$

in region I, where

$$\zeta_i^{(2)}=\frac{r_i(r_i^{(2)}-r_i)-2(r_i^{(1)})^2}{(-r_i^{(1)}\cos\theta_i+r_i\sin\theta_i)^3} \tag{4.18b}$$

and

$$\zeta_i^{(1)}=\frac{r_i^{(1)}\sin\theta_i+r_i\cos\theta_i}{-r_i^{(1)}\cos\theta_i+r_i\sin\theta_i}\ . \tag{4.18c}$$

### C. Newton method and comparison with an exact analytical solution

Next to solve (4.11) we use an $n$-dimensional Newton method. Given the $n$ vector of unknowns at the $m$th iteration $\underline{w}^m=\{w_1^m,\ldots,w_n^m\}$ and the $n$ vector $\underline{g}^m=\{g_1^m(\underline{w}^m),\ldots,g_n^m(\underline{w}^m)\}$, $\underline{w}^*$ which solves $\underline{g}(\underline{w}^*)=0$ is found recursively to arbitrary accuracy by solving the linear system

$$[J]\Delta\underline{w}=\underline{g}^m\ , \tag{4.19}$$

where $[J]$ is the Jacobian $[J]_{ij}=(\partial g_i^m/\partial w_j^m)$, and then repeating the procedure with

$$\underline{w}^{m+1}=\underline{w}^m-\Delta\underline{w} \tag{4.20}$$

as initial guess. Here we calculate $[J]$ numerically and solve (4.19) using a linear algebra subroutine of the Port Library. All computations are performed on a Ridge computer. The vector $\underline{g}$, defined by (4.11) for $i=1$ through $n$, depends only on $P,r_1,\ldots,r_n$, and the fictitious point $r_{n+1}$ which corresponds to the continuation of the interface at $\theta=(\pi/2)+h_1$, this point being introduced in order to evaluate $r_n^{(1)},r_n^{(2)}$ (and therefore the tip curvature $\kappa_n$), and $r_{n-1}^{(3)}$ by central differences. We fix $r_n=\frac{1}{2}$ and for given values of $n$ and $b$ choose $l$ as the integer part of $(4nb+\pi)/(4b+\pi)$. This choice for $l$ ensures $r_lh_1\simeq\frac{1}{2}h_1\simeq h_2$ at $\theta=0$, and distributes the grid points evenly between the two regions (I and II). The absolute height of the interface is arbitrary and $\zeta_1$ is chosen such that $\zeta_{\rm tip}=0$. Finally we need to specify the $n$ unknowns $(\underline{w})$. This is done in two different ways.

#### 1. Zero slope BC's

In this method we impose zero slope BC's at the tip of the cell (which implies $r_{n+1}=r_{n-1}$ in central differences) and let the dimensionless cell spacing $P$ become an unknown to be determined together with the shape of the interface in the Newton method. The $n$ vector of unknowns is then

$$\underline{w}=[r_1,\ldots,r_{n-1},P],\quad\text{with } r_{n+1}=r_{n-1}\ . \tag{4.21}$$

#### 2. Finite cusp BC's

In this method[4,5,9] $P$ is fixed but the zero slope BC's is relaxed in which case $r_{n+1}$ becomes an unknown. In this case

$$\underline{w}=[r_1,\ldots,r_{n-1},r_{n+1}]\ , \tag{4.22}$$

with fixed $P$. The magnitude of the cusp at the tip $[(dr/d\theta)]_{\rm tip}=r_n^{(1)}$ is calculated for several values of $P$ and the zero crossings of $[(dr/d\theta)]_{\rm tip}$ versus $P$ determine the physically admissible singular solutions. The advantage of this method is that more than one solution can be found while method (1) is more efficient to follow a branch of solutions as function of a control parameter, the dimensionless velocity $V$ in the present case.

To check our code we first make contact with the exact analytical solution for zero surface tension Saffman-Taylor fingers.[7] Accordingly we set $\sigma=0$ and substitute in (4.11) the expressions (4.8b), (4.8c), and (4.9) evaluated in the $P\to 0$ limit. As discussed at the end of Sec. II, this solution is simply the planar interface (a trivial shape) in the limit where the finger fills the channel. To check our code against a nontrivial shape we perform the additional transformations

$$\begin{aligned}&\Delta\zeta\to a^{-1}\Delta\bar{\zeta}\ ,\\ &(x-x')\to a^{-1}(\bar{x}-\bar{x}')\ ,\\ &(x+x')\to a^{-1}(\bar{x}+\bar{x}'-1)\ ,\end{aligned} \tag{4.23}$$

in (2.18) [and their equivalents in (4.11)]. Equation (2.18) then describes the shape of a viscous finger of width unity with the endpoint singularity at $\bar{x}=0$ and the wall of the channel at $\bar{x}=(1-a)/2$. By symmetry the other endpoint is at $\bar{x}=1$ and the other wall at $\bar{x}=(1+a)/2$. The exact shape of the finger in this parametrization is then given by

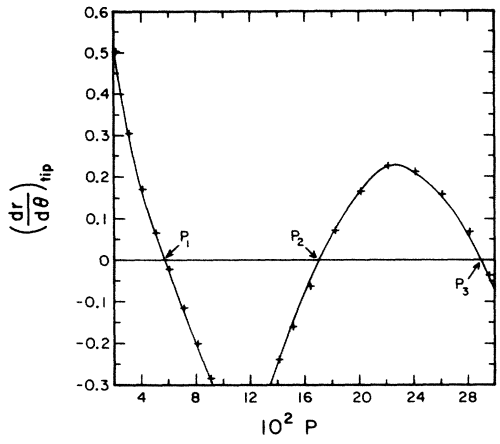


FIG. 1. $(dr/d\theta)_{tip}$ vs $P$ for $V=10^{-4}$; the zero crossings are at $P_1=5.75\times10^{-2}$, $P_2=0.176$, and $P_3=0.297$.

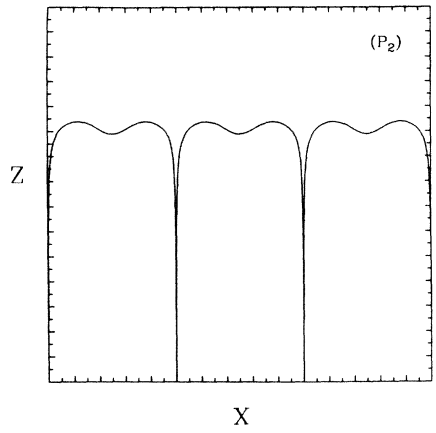


FIG. 3. Higher-order solution corresponding to $P_2$.

$$\bar{\zeta}_s(\bar{x})=\frac{a-1}{\pi}\ln\sin(\pi\bar{x})\ . \tag{4.24}$$

Starting from smooth but arbitrary initial conditions with $b=1$ and $n=60$ we found convergence to (4.24) for different values of $a$, with several significant figures of accuracy, in 6—10 iterations of the Newton method, the iterations being stopped when

$$\left[\frac{1}{n}\sum_{i=1}^{n}(g_i)^2\right]^{1/2}<10^{-10}\ .$$

## V. RESULTS AND DISCUSSION

To investigate (2.18) for $\sigma\neq0$ we first chose $V=10^{-4}$ and calculated $(dr/d\theta)_{tip}$ for several values of the dimensionless cell spacing $P$ using the finite cusp BC's method (4.22) described in Sec. IV. We used typically 40—80 grid points and values of $b$ between one and two (recall that $b=\zeta_l-\zeta_1$ is the length of region II). The results are plotted in Fig. 1 showing the first three-zero crossing at $P_1=5.75\times10^{-2}$, $P_2=0.176$, and $P_3=0.297$. For each zero crossing the result is then checked by repeating the calculation with the zero-slope BC's method (4.21). The two methods are found to yield the same values of $P_i$. The interfaces corresponding to $P_1$, $P_2$, and $P_3$ are shown in Figs. 2, 3, and 4, respectively. Note that $P_2$ and $P_3$ are nearly odd integer multiples of $P_1$, each integer also giving the number of extrema (points of zero slope per cell) in the corresponding pattern. We have $P_2/P_1=3.06\simeq3$ and $P_3/P_1=5.17\simeq5$ with accordingly 3 and 5 extrema in Figs. 3 and 4, respectively. This indicates a clear connection between the value of the cell spacing and the morphology of the cell, with $P_1$ setting the length scale of oscillations in the interface profile. In addition as $P_i$ increases the amplitude of the pattern in the tip region decreases. This can be understood if we note that $\sigma_i=V/P_i^2$ decreases with increasing $P_i$ and that steady-state solutions must therefore approach the planar interface as $\sigma_i\to0$ (see the discussion at the end of Sec. II). It is even likely that this structure persists to higher values of $P_i$ (smaller values of $\sigma_i$), beyond the first three values calculated here, with a possibly infinite sequence of higher-order steady-state solutions characterized by a decreasing amplitude (apart from the endpoint singularities)

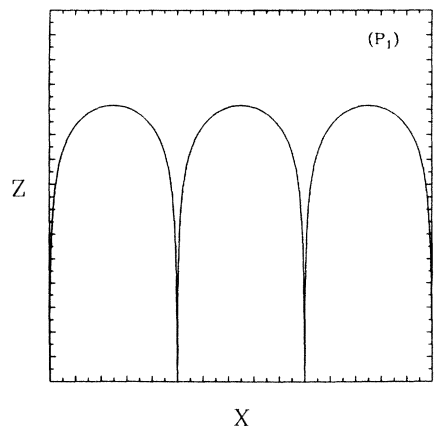


FIG. 2. Finger solution corresponding to $P_1$; $X$ and $Z$ are measured in units of the cell spacing $\lambda_i$, with $i=1$, 2, and 3 in Figs. 2, 3, and 4, respectively.

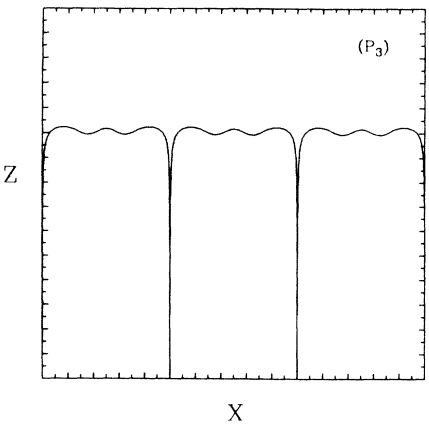


FIG. 4. Higher-order solution corresponding to $P_3$.

and an increasing number of oscillations as $\sigma_i \to 0$.

Next the exponential behavior of solutions near the endpoint singularity was investigated as a self-consistency check of the analytical predictions of Sec. III. For this purpose we have plotted in Fig. 5

$$f_1(\zeta) \equiv \frac{dx}{d\zeta} \Big/ x(\zeta)$$

and

$$f_2(\zeta) \equiv \frac{d^2x}{d\zeta^2} \Big/ \frac{dx}{d\zeta}$$

versus $\zeta$ in the range $\zeta_1 \le \zeta \le \zeta_l$ (region II) for the interface of Fig. 2 corresponding to $\sigma = V/P_1^2 = 3\times 10^{-2}$. In the asymptotic regime it follows from (3.5) that $f_1(\zeta) = f_2(\zeta) = t$ with $t$ given by the root of (3.12); for $\sigma = 3\times 10^{-2}$, $t = 2.45$. Figure 5 shows the crossover of the interface profile in the asymptotic regime with a decay rate $t$ in excellent agreement with the analytical prediction ($t = 2.45$). Note a slight discrepancy between the values of $t$ determined by $f_1$, and $f_2$ which reflects a decrease in numerical accuracy for higher derivatives. For smaller values of $\sigma_i$ ($i = 2,3$) we also found good agreement with (3.12), $t \to \pi$ as $\sigma_i$ decreases.

The small-$P$ dependence of $\sigma_1$, the value of $\sigma$ corresponding to the finger solution of Fig. 2, was then studied by using the zero-slope BC's method and calculating $P_1$ and $\sigma_1 = (V/P_1^2)$ for several values of $V$ over four decades $10^{-6} \le V \le 10^{-2}$. A plot of $\sigma_1$ versus $P_1$ is shown in Fig. 6 indicating that $\sigma_1$ varies relatively slowly with $P_1$. Consequently the integral equation (2.20) and the scaling of $\lambda_1$ given by (2.21) remain quantitatively accurate up to values of Peclet number $P_1$ of about 0.1, corresponding to dimensionless velocities $V$ of order $10^{-3}$. [Here the value of $\sigma_1$ determined by (2.20) is the $P_1 = 0$ crossing of the curve in Fig. 6.] In addition the dependence of the shape of the finger solution on Peclet number was found to be very weak with, on the scale of Fig. 2, the finger solutions corresponding to values of $P_1$ between $5.7\times 10^{-3}$ (for $V = 10^{-6}$) and $P_1 = 0.64$ (for $V = 10^{-2}$) being nearly indistinguishable.

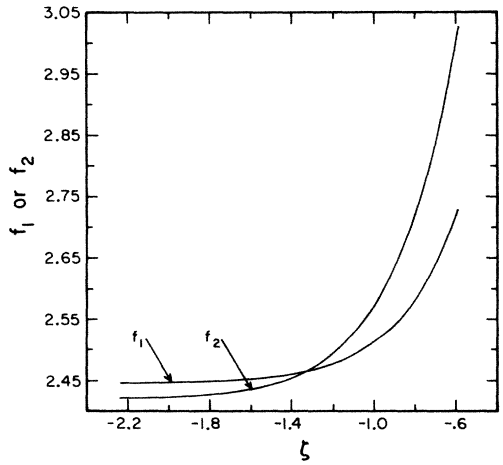


FIG. 5. Plot of $f_1(\zeta) \equiv (dx/d\zeta)/x(\zeta)$ and $f_2(\zeta) \equiv (d^2x/d\zeta^2)/(dx/d\zeta)$ vs $\zeta$, $\zeta_1 \le \zeta \le \zeta_l$, for the finger solution of Fig. 2 ($\zeta_{\text{tip}} = 0$). Note that the asymptotic behavior of the interface profile is consistent with an exponential solution.

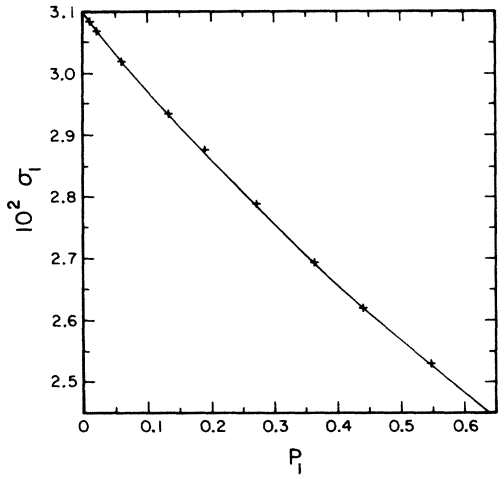


FIG. 6. Effective surface tension $\sigma_1$ vs solute Peclet number $P_1$ (the index 1 refers to the finger solution of Fig. 2).

In terms of solidification in a channel of fixed width $\lambda$ the problem becomes one of velocity selection. The finger solution (Fig. 2) with the largest value of $\sigma$ then corresponds to the state with the smallest velocity [i.e., $\sigma \propto (d_0 l/\lambda^2)$ and $l = (2D/v)$]. This situation differs from dendritic growth where, for $\Delta \neq 1$, the selected state corresponds to the needle crystal solution with the largest velocity. (As shown in Ref. 28 this solution becomes planar in the limit $\Delta \to 1$.) To see how this difference comes about, we first note that, for dendrites, the selected state also corresponds to the state with the largest value of $\sigma \propto (d_0 l/\rho^2)$, where $\rho$, the tip radius, is the analog of $\lambda$. However, the largest value of $\sigma$ does not correspond in this case to the largest value of $l$ because the ratio $(\rho/l)$ (the Peclet number) is fixed by the undercooling $\Delta$. Then $\sigma \propto [d_0/\rho P(\Delta)]$ is maximum when $\rho$ and therefore $l$ are minima (within the discrete set of needle crystals).

Also in connection with solidification in a channel our present study could easily be extended to values of $\Delta = (C_\alpha - C_\infty)/\Delta C^0$ less than unity. Here we have focused our study on the limit of unit undercooling primarily because this limit (where the finger fills the channel) is most relevant to directional solidification. When $\Delta < 1$ it is easy to show that overall solute conservation requires that the ratio of the width of the finger to the width of the channel must equal $\Delta$. Then the zero surface tension steady state in the $P \to 0$ limit is simply the Saffman-Taylor finger given by (4.24) with $a = (1/\Delta)$ [for a finger of unit width in a channel of width $a = (1/\Delta)$]. At finite surface tension it is reasonable to expect a discrete set of steady states. Furthermore the value of $\sigma$ corresponding to a fingerlike solution in the $P \to 0$ limit, $\sigma_1(\Delta)$, should decrease with decreasing $\Delta$, this behavior being strongly suggested by the analogy with the Saffman-Taylor problem[8-12] where $\sigma_1(\Delta) \to 0$ when $\Delta \to \frac{1}{2}$.

To conclude this section it is interesting to observe that

$$\lambda_s/\lambda_i = 4\pi(\sigma_i)^{1/2}$$

equals 2.18, 0.71, and 0.42 for $i=1$, 2, and 3, respectively, where $\lambda_s = 2\pi(d_0 l)^{1/2}$ is the stability length of the plane interface.[29] Therefore the finger solution of Fig. 2 lays outside the band of unstable wave numbers of the plane, with a finger width nearly half the stability length, while the higher order solutions of Figs. 3 and 4 lay within this band. The relative stability of these different solutions is discussed qualitatively in our concluding remarks.

## VI. CONCLUDING REMARKS

In conclusion we have analyzed singular cells in the small Peclet number limit of the simplest nonlocal model of solidification (symmetric model at unit undercooling) and shown that, at fixed velocity and finite surface tension, these states can only exist for a discrete set of values of the cell spacing $\lambda$, where $\lambda$ scales as $(d_0 l)^{1/2}$ in this limit; at zero surface tension the only steady state is the planar interface.

Interestingly, steady-state singular cells and dendrites in the symmetric model are very similar in that, at finite surface tension, they both belong to discrete sets of states. However, they differ significantly in that, for dendrites, the finite surface tension state with the largest velocity lays near one member of an underlying zero surface tension family of steady states (the Ivantsov family), while for cells at unit undercooling the finger and planar solutions are far apart. This difference indicates that—unfortunately—the analytical methods developed recently to study dendritic crystals or Saffman-Taylor fingers at small surface tension (the limit where the width of the finger is half the channel width) can not be used directly for singular cells.

With regard to the stability of these states the finger solution is likely to be the only stable steady state, the higher-order solutions (with multiple oscillations) being locally unstable against tip splitting. This, of course, is for the solidification of a *single* finger at unit undercooling in a channel of width $\lambda$. In connection with directional solidification, an *array* of fingers in the absence of temperature gradient is likely to suffer a global instability where one finger moves ahead of the solidification front, enhancing its growth rate at the expense of its neighbors. Thus, although model A has provided us with a simple starting point to study solidification fingers and has helped us gain insight in the small Peclet number limit, it fails to describe the important coupling between the temperature and solute fields, this coupling playing a crucial role in the global stability of a cellular array. In light of this, it would be interesting to next elucidate how much of the structure of singular solutions revealed here (i.e., a discrete set of states) persists in the more realistic one-sided model of directional solidification which incorporates this coupling. Our preliminary results for the one-sided model indicate that a discrete set of singular cells persists, at least in the case of unit partition coefficient.[30]

## ACKNOWLEDGMENTS

I wish to thank Professor J. S. Langer, M. Marder, and D. Meiron for many valuable discussions. I have also benefited from helpful conversations with M. Cross, G. Milton, and M. Wilkinson. This material is based upon research supported by the California Institute of Technology through funds of the Weingart Foundation, the National Science Foundation under Grant No. DMR-8412543, and the U. S. Department of Energy under Grant No. DE-FG03-84ER45108.

[1] D. Kessler, J. Koplik, and H. Levine, Phys. Rev. A **31**, 1712 (1985).
[2] E. Ben-Jacob, N. Goldenfeld, B. G. Kotliar, and J. S. Langer, Phys. Rev. Lett. **53**, 2110 (1984).
[3] B. Caroli, C. Caroli, B. Roulet, and J. S. Langer, Phys. Rev. A **33**, 442 (1986).
[4] D. Meiron, Phys. Rev. A **33**, 2704 (1986).
[5] D. Kessler, J. Koplik, and H. Levine, Phys. Rev. A **33**, 3352 (1986).
[6] D. C. Hong and J. S. Langer Phys. Rev. A **34**, 1462 (1986).
[7] P. G. Saffman and G. I. Taylor, Proc. R. Soc. A **245**, 321 (1958).
[8] J. W. McLean and P. G. Saffman, J. Fluid Mech. **102**, 455 (1981).
[9] J. M. Vanden-Broeck, Phys. Fluids **26**, 2033 (1983).
[10] R. Combescot, T. Dombre, V. Hakim, Y. Pomeau, and A. Pumir, Phys. Rev. Lett. **56**, 2036 (1986).
[11] D. C. Hong and J. S. Langer, Phys. Rev. Lett. **56**, 2032 (1986).
[12] B. I. Shraiman, Phys. Rev. Lett. **56**, 2028 (1986).
[13] R. Trivedi, Met. Trans. **15A**, 977 (1984).
[14] H. Esaka and W. Kurz, J. Cryst. Growth **72**, 578 (1985).
[15] S. de Cheveigne, C. Guthmann, and M.-M. Lebrun, J. Cryst. Growth **73**, 242 (1985).
[16] D. J. Wollkind and L. A. Segel, Philos. Trans. R. Soc. London **51**, 268 (1970).
[17] J. S. Langer and L. A. Turski, Acta Metall. **25**, 1113 (1977).
[18] J. S. Langer, Acta Metall. **25**, 1121 (1977).
[19] G. Dee and R. Mathur, Phys. Rev. B **27**, 7073 (1983).
[20] A. Karma and N. Goldenfeld, Phys. Rev. B **31**, 7018 (1985).
[21] A. C. Newell and J. A. Whitehead, J. Fluid Mech. **38**, 279 (1969).
[22] L. A. Segel, J. Fluid Mech. **38**, 203 (1969).
[23] L. Hungar and R. Brown, Phys. Rev. B **31**, 5931 (1985).
[24] G. I. Sivashinsky, Physica (Amsterdam) **8D**, 243 (1983).
[25] M. Kerszberg, Phys. Lett. **105A**, 241 (1984).
[26] P. Pelcé and Y. Pomeau, Stud. Appl. Math. (to be published).
[27] *Table of Integrals, Series, and Products,* edited by I. S. Gradshteyn and I. M. Ryzhik (Academic, New York, 1980).
[28] D. C. Hong and J. S. Langer, Phys. Rev. A **34**, 1462 (1986).
[29] J. S. Langer, Rev. Mod. Phys. **52**, 1 (1980).
[30] A. Karma, Phys. Rev. Lett. **57**, 858 (1986).